A GAUSSIAN-RAYLEIGH MIXTURE MODELING APPROACH FOR THROUGH-THE-WALL RADAR IMAGE SEGMENTATION

Cher Hau Seng[⋆]*, Abdesselam Bouzerdoum*[⋆]*, Moeness G. Amin*[†] and *Fauzia Ahmad*[†]

[⋆]School of Electrical, Computer and Telecommunications Engineering, University of Wollongong, Wollongong, NSW 2522, Australia.
[†]Radar Imaging Lab, Centre for Advanced Communications, Villanova University, Villanova, PA 19085, USA.

ABSTRACT

In this paper, we propose a Gausssian-Rayleigh mixture modeling approach to segment indoor radar images in urban sensing applications. The performance of the proposed method is evaluated on real 2D polarimetric data. Experimental results show that the proposed method enhances image quality by distinguishing between target and clutter regions. The proposed method is also compared to an existing Neyman-Pearson (NP) target detector that has been recently devised for through-the-wall radar imaging. Performance evaluation of both methods shows that the proposed method outperforms the NP detector in enhancing the input images.

Index Terms— Through-the-Wall Radar, Target Detection, Image Segmentation, Mixture Modeling

1. INTRODUCTION

Segmentation of radar images is often performed with the ultimate goal to improve the image quality for subsequent analysis and scene description [1]. Generally, radar image segmentation is essential for applications such as target detection, classification, and identification. Since the detection of stationary targets behind walls has recently been a subject of interest in many applications related to rescue missions, homeland security, and defense [2, 3, 4], we investigate a mixture modeling-based image segmentation method for through-the-wall radar imaging (TWRI), which can also be applied as a target detection method.

The proposed method estimates the probability density function (PDF) of the image intensity using a mixture of Gaussian and Rayleigh distributions. Previous work presented in [5, 6] assumes that all target regions are Gaussian distributed and all clutter regions are Rayleigh distributed. The proposed method, on the other hand, models the PDF of the image intensity by using a mixture of Gaussian and Rayleigh distributions: the strong target regions and the weak clutter/noise regions are modeled with Rayleigh distributions, and the remaining regions as a multi-modal Gaussian mixture. The target regions are then extracted from the mixture model to produce an enhanced image, as well as to detect the targets.

The proposed mixture modeling-based image segmentation method is evaluated on real 2D polarimetric data collected in the Radar Imaging Lab, Center for Advanced Communications, Villanova University, USA. The performance is assessed in terms of the separation of target from clutter in individual images. The detection performance of the proposed method is compared to the Neyman-Pearson (NP) detector presented in [6]. Since both methods produce a binary image, the original image is masked to generate an enhanced image. The two methods are then compared based on their ability to enhance the input image, which is produced by frequency-domain backprojection. Experimental results show that the proposed image segmentation method outperforms the NP detector by providing a higher improvement factor in target-to-clutter-ratio.

The remainder of the paper is organized as follows. Section 2 details the NP detection method proposed in [6]. The proposed mixture modeling-based image segmentation method is then discussed in Section 3. Section 4 presents the experimental results depicting the performance of the proposed method in segmenting the polarimetric data. Comparison between the proposed method and the NP detector in terms of image enhancement is also discussed. Section 5 concludes the paper.

2. NEYMAN-PEARSON DETECTOR

In this section, we review the iterative pixel-wise NP detector proposed in [6], which adapts the test parameters to the radar image statistics. Let x be the observed pixel intensity from the acquired magnitude image I. Let H_0 and H_1 denote, respectively, the null (target absent) and alternative (target present)

[⋆]Emails: {aseng, a.bouzerdoum}@uow.edu.au.
[†]Emails: {moeness.amin, fauzia.ahmad}@villanova.edu.
The work by C.H. Seng and A. Bouzerdoum has been supported in part by the Australian Research Council. The work by M.G. Amin and F. Ahmad was supported in part by the US Army Research Lab contract W911NF-07-D-0001.

hypothesis. For a single image, the pixel-wise NP test is given as,

$$\frac{p(x|H_1)}{p(x|H_0)} \gtrless \gamma, \tag{1}$$

where the functions $p(\cdot|H_0)$ and $p(\cdot|H_1)$ are the conditional PDFs under the null and alternative hypothesis, which are assumed to be Rayleigh and Gaussian distributed, respectively. The parameter γ is the likelihood ratio threshold, which can be obtained by specifying a desired false alarm rate (FAR), α, as

$$\alpha = \int_{\gamma}^{\infty} P_\ell(\ell|H_0)d\ell, \tag{2}$$

where $P_\ell(\ell|H_0)$ denotes the distribution of the likelihood ratio under the null hypothesis. Let $\hat{\theta}^0_{H_0}$ and $\hat{\theta}^0_{H_1}$ denote the initial estimates of the parameter vectors θ_{H_0} and θ_{H_1} describing the PDFs under H_0 and H_1, respectively. Given a FAR α, a binary image B^1_{NP}, where superscript 1 represents the first iteration, can be obtained by evaluating (1). In order to optimize the estimation of the noise and test PDF parameters, morphological filtering is employed to obtain the binary image B^1_{MF} (see [7] for details). This image can then be used as a mask on the original image to obtain the revised parameter estimates $\hat{\theta}^1_{H_0}$ and $\hat{\theta}^1_{H_1}$. These revised parameters are then fed back to the NP test again to obtain an improved detection result. The iteration stops when convergence is achieved.

It is noted that the final output of the statistical detector described above is a single binary image that indicates the presence or absence of the targets.

3. PROPOSED SEGMENTATION METHOD

In the proposed method, we assume that the pixel values forming the image are multi-modal, where each mode in the histogram may correspond to a certain region in the image; for instance, the target, sidelobe, clutter, or noise region. Therefore, by appropriately modeling the image intensity distribution, the probabilities of any pixel value belonging to different regions can be found. Here, we apply the Gaussian and Rayleigh distributions to estimate the PDF. However, unlike the NP detector that assumes Gaussian distributed targets and Rayleigh distributed clutter, we propose a technique that models the PDF using a mixture of Gaussian and Rayleigh distributions. As an extension to the Gaussian mixture modeling-based segmentation [8], the proposed Gaussian-Rayleigh mixture modeling also uses the EM algorithm to maximize the likelihood estimate of the mixture parameters. The proposed multivariate PDF can be expressed as a weighted sum of k class conditional PDFs, given as

$$f(x) = \sum_{i=1}^{k} \omega_i f_i(x|\boldsymbol{\theta}_i). \tag{3}$$

where ω_i is the component weight and $\boldsymbol{\theta}_i$ consists of the mixture parameters. Empirical observations of radar images show that the lowest intensity pixels tend to belong to the clutter or background noise region, whereas the highest intensity levels tend to belong to target regions. Due to the high concentration of low pixel values and a low concentration of very high pixel values, the intensity distribution tends to peak at both extreme ends, as shown in Fig. 1.

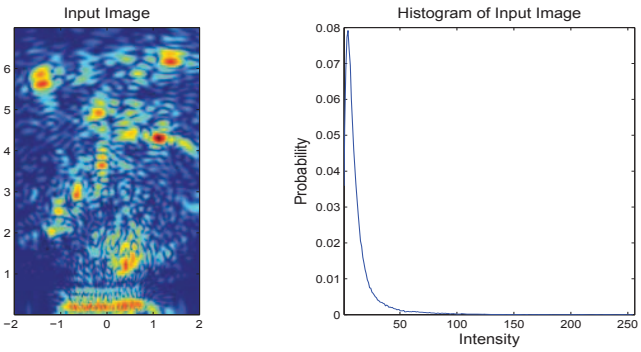

Fig. 1. Input image produced by the polarimetric data of a calibrated scene and its histogram.

Thus, the noise and clutter region with the lowest intensity levels and the target region with the highest intensity levels are modeled, in this paper, as Rayleigh distributions,

$$f_R(x) = \frac{x}{\sigma^2} \exp \frac{-x^2}{2\sigma^2}, \tag{4}$$

while the regions in between are modeled as Gaussian distributions

$$f_G(x) = \frac{1}{\sqrt{2\pi\sigma^2}} \exp \frac{-(x-\mu)^2}{2\sigma^2}, \tag{5}$$

where σ and μ denote the standard deviation and the mean of the distribution, respectively. Hence, the mixture parameters to be estimated are defined as $\boldsymbol{\theta_{R}}_i = (\sigma_i^2)$ and $\boldsymbol{\theta_{G}}_i = (\mu_i, \sigma_i^2)$ for the Rayleigh and Gaussian component distributions, respectively. Let x_n be the observed intensity from image I. The mixture parameters $\boldsymbol{\theta}$ for K mixture components can be automatically obtained as follows:

1. Let ν_k denote the covariance of the k-th component. Estimate the initial values of the mixture parameters, $\boldsymbol{\theta} = (\mu_2, \mu_3, ..., \mu_{K-1}; \nu_1, \nu_2, ..., \nu_K)$.
2. Compute the conditional PDF $f_k(x_n|\boldsymbol{\theta}_k)$ using the current estimated value of $\boldsymbol{\theta}$:

$$f_k(x_n|\boldsymbol{\theta}_k) = \begin{cases} \frac{x_n}{|\nu_k|} \exp \frac{-x_n^2}{2|\nu_k|}, & \text{if} \quad k = 1 \\ \frac{1}{\sqrt{2\pi|\nu_k|}} \exp \frac{-(x_n-\mu_k)^2}{2|\nu_k|}, & \text{if} \quad 1 < k < K \\ \frac{255-x_n}{|\nu_k|} \exp \frac{-(255-x_n)^2}{2|\nu_k|}, & \text{if} \quad k = K \end{cases} \tag{6}$$

3. Determine the posterior probability that a pixel x_n belongs to class k as:

$$\hat{h}_{k,n} = \frac{\omega_k f_k(x_n|\boldsymbol{\theta}_k)}{\sum_{k=1}^{K} w_k f_k(x_n|\boldsymbol{\theta}_k)}, \tag{7}$$

for $k = 1, 2, ..., K$ and $n = 1, 2, ..., N$, where N is the total number of pixels in the image.

4. Update the component weight by averaging the posterior probabilities of each class:

$$\hat{w}_k = \frac{1}{N} \sum_{n=1}^{N} \hat{h}_{k,n}. \tag{8}$$

5. Update parameter vector $\boldsymbol{\theta}$:

$$\hat{\mu}_k = \frac{1}{N} \sum_{n=1}^{N} \frac{\hat{h}_{k,n} x_n}{\hat{w}_k}, \qquad \text{if} \quad 1 < k < K \tag{9}$$

$$\hat{\nu}_k = \begin{cases} \frac{1}{N} \sum_{n=1}^{N} \frac{\hat{h}_{k,n} x_n^2}{\hat{w}_k}, & \text{if} \quad k = 1, k = K \\ \frac{1}{N} \sum_{n=1}^{N} \frac{\hat{h}_{k,n} (x_n - \hat{\mu}_k)^2}{\hat{w}_k}, & \text{if} \quad 1 < k < K \end{cases} \tag{10}$$

6. Iterate Steps 2 to 5 until the relative changes in the mixture parameter estimates are smaller than a tolerance, ε.

In the proposed method, $\sigma_k = \sqrt{\hat{\nu}_k}$ and the pixel x_n is assigned to the class that produces the highest $\hat{h}_{k,n}$. In the sequel, ε is set to 10^{-5}. When the number of mixture components *K* is small, the mixtures model may not satisfactorily fit the intensity range of the input image. However, a large *K* tends to over-fit, introducing more mixture components than required. Hence, the optimal number of mixture components is determined through the minimization of the Bayesian information criterion (BIC) [8]:

$$\beta = -2 \sum_{n=1}^{N} \log_{10} \left[f(x_n | \boldsymbol{\theta}) \right] + K \log_{10} (N). \tag{11}$$

As it was empirically observed that the last two components with the highest intensity values belong to the target region, these regions are extracted to form the binary mask that depicts target presence.

4. EXPERIMENTAL RESULTS

We evaluate the proposed mixture modeling-based image segmentation method on real 2D polarimetric data collected in the Radar Imaging Lab, Center for Advanced Communications, Villanova University, USA. Both co-polarization (HH and VV) and cross-polarization (HV) data sets were collected from a calibrated scene, containing a sphere, a top hat, a vertical dihedral, two dihedrals rotated at 22.5 and 45 degrees, respectively, and two trihedrals, all placed at different downrange, cross-range and elevation bins, as shown in Fig. 2. For each polarization setting, the scene is imaged with a 1 GHz waveform bandwidth centered at 2.5 GHz through a non-homogeneous plywood and gypsum board wall using a 57-element linear synthetic aperture with an inter-element spacing of 22 mm. We note that all radar images presented, other than the binary ones, are plotted on a 35 dB log scale,

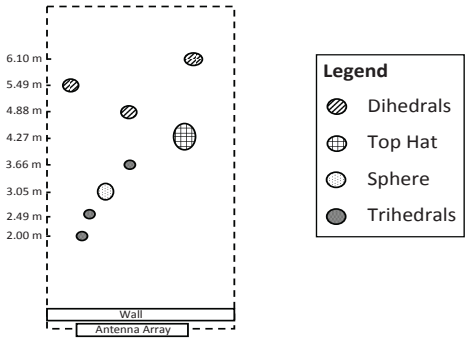

Fig. 2. Schematic of the calibrated scene.

and the vertical and the horizontal axes represent the downrange and cross-range, respectively, with units in meters.

The three input images corresponding to the calibrated scene are provided in the top row of Fig. 3. It can be observed that only two targets are detected in the HV image. This is due to the fact that the rotated dihedrals produce a stronger cross-polarization return. The middle row of Fig. 3 shows the image segmentation results of evaluating the proposed method on the three input images. The optimal number of mixture components for HH, HV and VV, determined through the BIC, are 10, 11, and 12, respectively. It can be observed that the proposed method successfully maintained most of the targets while suppressing clutter; although there were some missed detections.

For comparison purposes, the NP detector with 2.5% FAR is also applied to the three input images (bottom row of Fig. 3). We observe that the NP detector under-segments the input images by detecting both targets and clutter. In addition, the detected clutter levels are much higher than that of the proposed method. Thus, noise and clutter present in the original images persist even after application of the NP detector.

Since both the proposed method and the NP detector generate a binary image, the original image is masked using the binary output to produce an enhanced image that only consists of the target regions. The image enhancements achieved by the two methods are compared in terms of the Improvement Factor in the Target-to-Clutter Ratio, denoted as IF. Let $\mathcal{P}_{\mathcal{R},I}$ denote the average power of region $\mathcal{R}$ in image I. The IF is then given as

$$\text{IF} = 10 \log_{10} \left[\frac{\mathcal{P}_{t,out} \times \mathcal{P}_{c,in}}{\mathcal{P}_{t,in} \times \mathcal{P}_{c,out}} \right]. \tag{12}$$

$\mathcal{P}_{r,m}$ can be expressed as

$$\mathcal{P}_{r,m} = \frac{1}{N_r} \sum_{(x,y) \in r} I_m(x,y)^2, \tag{13}$$

where $I_m(x,y)$ is the pixel located at coordinates (x,y) in region r, and N_r is the number of pixels in that region. The subscripts t, c, in, and out denote the target region, clutter region, input image and output image, respectively.

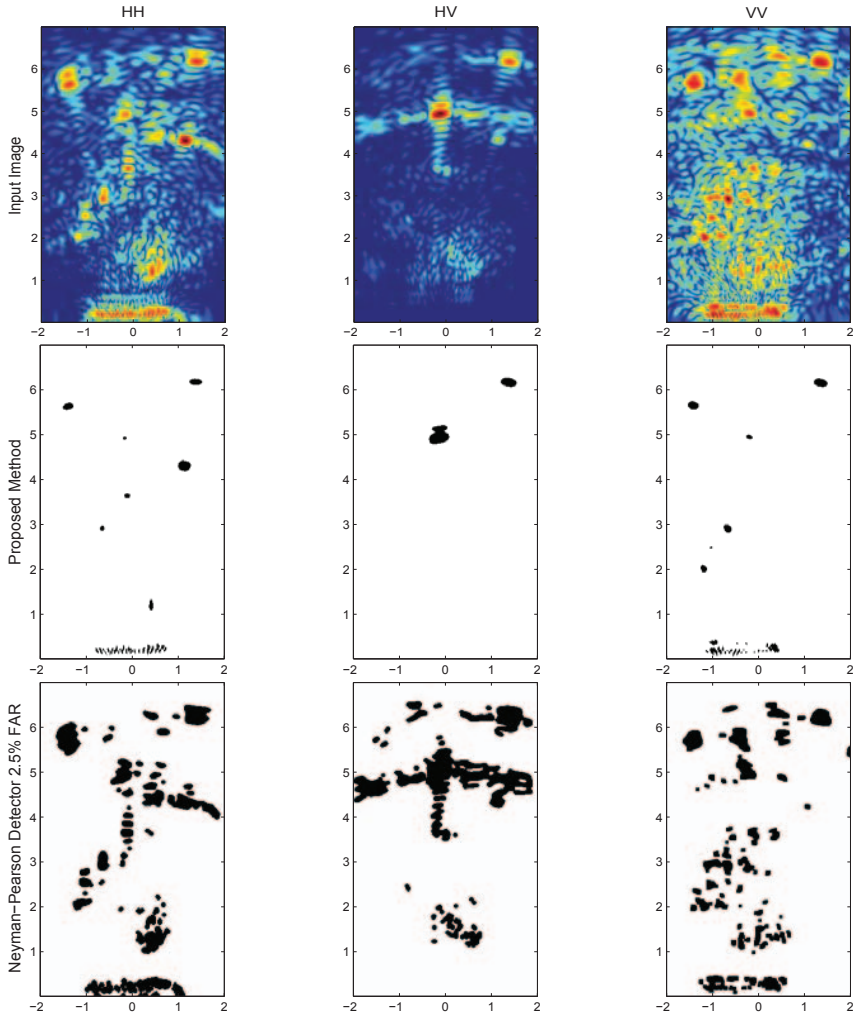

Fig. 3. Experimental results showing, from top to bottom, the images of a calibrated scene, the image segmentation results from the proposed method, and the target detection results by the NP detector.

It can be observed from Table 1 that the the proposed method outperforms the NP detector by producing enhanced images with a higher IF.

Table 1. Improvement Factor in Target-to-Clutter Ratio after Image Enhancements

	NP detector	**Proposed Method**
HH	1.9626	4.3735
HV	2.5142	17.7317
VV	3.0413	6.5480

5. CONCLUSION

In this paper, we proposed a new mixture modeling-based image segmentation method for TWRI, which models the PDF of an image using a mixture of Gaussian and Rayleigh distributions. Performances of the proposed approach was evaluated on real data. The proposed method was also compared to an existing NP target detector. Experimental results showed that the proposed method outperforms the NP detector in enhancing the images by better distinguishing between target and clutter.

6. REFERENCES

[1] J. Lee and I. Jurkevich, "Segmentation of SAR images," *IEEE Trans. Geosci. Rem. Sens.*, vol. 27, no. 6, pp. 674–680, 1989.

[2] M. Amin, *Through the Wall Radar Imaging*, CRC Press, 2010.

[3] F. Ahmad and M. Amin, "Multi-location wideband synthetic aperture imaging for urban sensing appl.," *J. Franklin Inst.*, vol. 345, no. 6, pp. 618–639, 2008.

[4] E. Baranoski, "Through wall imaging: Historical perspective and future directions," in *Proc. IEEE Intl. Conf. Acoust. Speech Signal Process.*, 2008, pp. 5173–5176.

[5] C. Debes, A. Zoubir, and M. Amin, "Target detection in multiple-viewing through-the-wall radar imaging," in *Proc. IEEE Intl. Geosci. Rem. Sens. Symp.*, 2008, pp. 173–176.

[6] C. Debes, M. Amin, and A. Zoubir, "Target detection in single- and multiple-view through-the-wall radar imaging," *IEEE Trans. Geosci. Rem. Sens.*, vol. 47, no. 5, pp. 1349–1361, 2009.

[7] C. Debes, J. Riedler, A. Zoubir, and M. Amin, "Adaptive target detection with appl. to through-the-wall radar imaging," *IEEE Trans. Signal Process.*, vol. 58, no. 11, pp. 5572–5583, 2010.

[8] O. Demirkaya, M. Asyali, and P. Sahoo, *Image Process. with MATLAB Appl. in Med. and Biol.*, CRC Press, 2008.